IOP Conf. Series: Materials Science and Engineering **397** (2018) 012028 doi:10.1088/1757-899X/397/1/012028

# Impact test of composite sandwich beam with built-in FBG sensor

**Haiping Pei, Yingying Wei, Yongzhen Chen, Li Wan[1]and Weiqing Liu**

Department of civil engineering, Nanjing Tech university, No 30, Puzhu Road(s), Nanjing, China.
Email: wanli@njtech.edu.cn

**Abstract.** Paulownia-wood composite sandwich beams were fabricated, in which FBG sensors were embedded in the grooves arranged on the top and bottom of paulownia wood core material. Four-point bending test, low-speed impact test and residual bending capacity test were carried out on the sandwich beams. In the bending test, comparative analysis of the built-in FBG sensor and externally attached resistance strain gauges showed that, with the characteristics of high sensitivity and accuracy, FBG sensor could reflect the total deformation behavior of the sandwich beams. In the low-velocity impact tests, FBG can effectively monitor the internal strain of the sandwich beam. However, due to the low acquisition frequency of instrument equipment, the details of the impact could not be reflected clearly. After impact, some available FBG sensors left in the beams could be used to evaluate the residual bearing capacity of the sandwich beam.

## 1. Introduction

With the high specific strength and specific rigidity, composite sandwich structures can be applied to the fields of road transportation, rail transportation, and aviation [1-3]. The composite sandwich structure is vulnerable to low-speed impact loads when they were produced and used, resulting in internal damage. And in turn leads to a significant reduction in its mechanical properties, which can cause safety hazards[4-7]. Therefore, it is extremely important to monitor the internal damage of composite sandwich structures for timely repair and replacement.

Compared with the ray, ultrasonic, infrared imaging and other damage detection methods commonly used at present, the FBG sensor has good compatibility with materials and monitoring, and has the advantages of small size, light weight, and high sensitivity. Also the amount of information collected can be detected internal damage in time. Fiber Bragg Gratings (FBGs) are spatially phased gratings that are formed within the core. The essence of the function is to form a narrowband (transmissive or reflective) filter or mirror in the core. The FBG sensor manufactured using this feature can change the wavelength of the reflected light wave according to changes in ambient temperature or strain. When the external strain acts on the FBG, its center wavelength drifts. According to the drift caused by each micro-strain, the wavelength conversion micro-strain formula can be obtained [8]:

$$\mu_t = (\lambda_t - \lambda_0) \times 1000 \div 1.2 \quad (1)$$

Where $\mu_t$ is the micro-strain at time $t$, $\lambda_t$ isthe center wavelength measured at time $t$, and $\lambda_0$ is the corresponding center wavelength of the fiber grating.

Domestic and foreign scholars have done a lot of research on the low-speed impact of composite sandwich structures. In 2000, Anderson and Madenci [9] studied the mechanical behavior of a

composite sandwich structure using foam and honeycomb as core material under impact load. Finally, it was found that the smaller the impact load is, the smaller the surface damage of the sandwich structure is. As the impact energy increases, the sag becomes larger and there is a center-to-edge diffusion crack on the impact panel. In 2012, Zhang Guangcheng et al [10] conducted impact tests on foam core and honeycomb core sandwich structures respectively. The results showed that members with PMI foam as the core exhibited better performance. With the treatment of slots and stitches resulted in PMI foam, the strength, stiffness, and interfacial properties of the sandwich members are further enhanced, and the impact bearing capacity is also significantly improved. In 2012, Hazizan [11] found that the impact damage first started at the interface between the panel and the sandwich on the basis of Herupa's research. The damage of the interface is a precipitating factor for panel delamination, core damage, etc, and therefore the research process for low speed impact. It is very necessary to study the interface properties. In 2002, Bai Remixing et al [12] studied the damage of the specimen after impact, and analyzed the impact of the residual compressive strength and tensile strength. In 2013, Dariusu and Sadighi[13] studied the bending performance of sandwich beams with fiber metal as the panel and compared them with sandwich beams with fiber/resin as the panel. The tests showed that the former performed better.

In this paper, a paulownia-wood composite sandwich beam embedded with FBG sensor is prepared, and an FBG sensor is embedded below the paulownia wood core material. The four-point static bending test, low-speed impact performance test, and residual bearing capacity test after impact were performed on the sandwich beam. The wavelength measured by the FBG sensor was converted to micro-strain, and compared with the value measured by the resistance strain gauge sensor, the load-strain relationship was obtained, real-time monitoring of the structural working status was realized. And the remaining bending bearing capacity of the sandwich beam was evaluated at the same time.

## 2. Test objects and Test Methods

### *2.1. Preparation of Specimen*

Composite sandwich beams were made of paulownia wood core material and alkali-free fiberglass cloth laid on the top and bottom through vacuum induction molding process. The paulownia wood core material was cut according to the specifications and dimensions of the test piece. A 2mm (width) 3mm (deep) groove was opened longitudinally at the center position of the wood core beam in the width direction. The FBG fiber grating sensor was laid in the groove and the cyanoacrylate adhesive was used. Initially fixed, spread four layers of fiber cloth and evenly coated unsaturated polyester resin with a brush. The sandwich beam structure is shown in Figure 1.

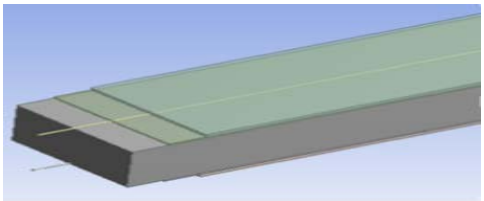

**Figure1.** Built-in FBG composite sandwich structure.

The fiber cloth adopts a biaxial E-type alkali-free glass fiber cloth with a density of 800 g/m $^2$ , the laying angle is 0°/90°, the fiber aspect ratio is 1:1, the thickness of the four-layer fiber cloth is 3.16 mm. Paulownia wood core is 340mm×60mm×20mm with a span of 300mm. The sandwich beam members used in the test were made by hand lay-up.

### *2.2. Specimen Parameters and Material Mechanical Properties*

According to the specification [14-15], the basic parameters of the test specimen are shown in Table 1. The basic mechanical properties of the test specimen are shown in Table 2.

**Table 1.** Detailed list of the specimen (Unite: mm)

| Type | Length /mm | Span /mm | Width /mm | Core thickness /mm | Number of layers | Specimen thickness /mm |
|---|---|---|---|---|---|---|
| FSSF-300 | 340 | 300 | 60 | 20 | 4 | 26.3 |

**Table 2.** Mechanical properties of materials

| Materials | Tensile Strength /MPa | Shear strength/ MPa | Elastic Modulus /GPa | Shear Modulus /GPa |
|---|---|---|---|---|
| Paulownia wood | 49.2 | 3.5 | 4.3 | 0.3 |
| Fiber/resin panel | 378 | -- | 8.9 | -- |

*2.3. Four-Point Bending Test*

The test is based on ASTM C393 "Standard Test Method for Flexural Properties of Sandwich Constructions"[16] and GB/T 1446 "Test Method for Bendability of Sandwich Structures"[17]. The dimensions of the test pieces are shown in Table 1 and the equipment uses a 50kN electro-hydraulic servo universal test. The machine is shown in Figure 3, equipped with a four-point fixture. The top of the ballast head and both ends of the support structure are hemispherical with a diameter of 20 mm. The distance between the two ballast heads is 100mm, and the distance between the support structures at both ends is 300mm.

Strain gauge placement layout shown in Figure 2.

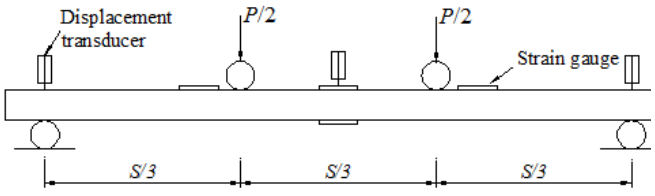


**Figure 2.** Strain gauge arrangement.

**Figure 3.** Test apparatus.

Displacement loading was used during the test. The loading speed was 2 mm / min. The position of the upper and lower clamps and specimens was adjusted to ensure that the applied line load was perpendicular to the specimen and the force at the two loading points was equal. The specimens were loaded to a deflection of 1/30 of the span, then unloaded and reloaded, and the loading and unloading repeated three times. In the test process, the strain gages and FBG strains are used to acquire the strain gages. The strain gages acquisition system adopts the Hepton dynamic acquisition system. The FBG sensor is connected to the SM125 fiber grating dynamic demodulator, and the acquisition frequency is 1000 Hz.

During the first loading, the test piece continued to emit a weak “creak” sound, the composite fiber panels at the loading point and the support all turned white. The bulge and debonding of the panel and the core material at the left loading point occurred. The base body is slightly crushed and the specimen is deformed and these were restored after unloading. During the second loading, the specimen initially emits a weak “click” sound. As the load increases, the sound becomes louder. The debonding phenomenon occurs on both sides of the panel and the core material at both loading points. The whitening degree of the loading on the upper panel was increased. The resin matrix was slightly cracked, and some residual deformation was observed after the sample was unloaded. During the third time loading, the sound became significantly larger. The damage of the panel and the resin matrix is obvious, and the panel is buckling. The residual deformation of the specimen after unloading increases compared with the second loading and unloading. The test failure phenomenon is shown in Figure 4.

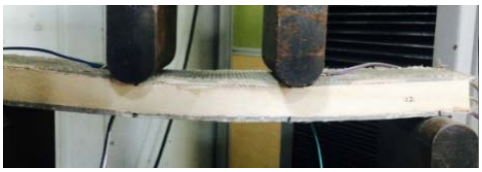

(a) First loading

(b) Second loading

(c) Third loading

**Figure 4.** Failure mode of bending test.

*2.4. Low Speed Impact Test*

According to the standard ASTM D7136 "Standard test method for measuring the damage resistance of a fiber-reinforced polymer matrix composite to a drop-weight impact event"[18], low speed impact test is performed. The test instrument is DTM1203 series drop hammer impact tester; punch is a hemispherical hammer with a diameter of 16mm and a mass of 5.5kg. The drop hammer falls freely from a certain height, the relevant data is collected by the hammer internal sensor to analyze the impact resistance. The hammer was dropped from heights of 400mm, 600mm, 800mm, 1000mm, and 1200mm to represent different impact energies by the control system setting parameters. The data was collected by computer, and the damage of the surface of the mixed sandwich beam was observed. Loading device shown in Figure 5, test parameters see Table 3.

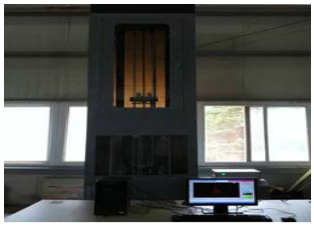

**Figure 5.** Experimental setup of low-velocity impact test.

**Table 3.** Detailed list of the specimen.

| Type | Length /mm | Span /mm | Width /mm | Core thickness /mm | Drop height /mm |
|---|---|---|---|---|---|
| AH-400 | 340 | 300 | 60 | 20 | 400 |
| AH-600 | 340 | 300 | 60 | 20 | 600 |
| AH-800 | 340 | 300 | 60 | 20 | 800 |
| AH-1000 | 340 | 300 | 60 | 20 | 1000 |
| AH-1200 | 340 | 300 | 60 | 20 | 1200 |

The duration of the impact process is relatively short, about 10ms or so. A “bang”, with a slight tearing of the fiber during the period, 400mm drop height, a small round pit at the impact point, the resin matrix due to extrusion White was oval. Starting from a height of 600 mm, the area of the whitening area increased with the increase of energy, and the shape of the whitening area also changed from an ellipse at a lower energy level to a larger one. There were two parallel cracks along the end of the line along the gods. Under high energy impact, the fiber cloth tore severely along the horizontal

lines, leading to cracking of the resin matrix. There was almost no damage on the lower surface, and the impact energy was less likely to propagate down the surface and was dissipated. The destruction of the specimen is shown in Figure 6.

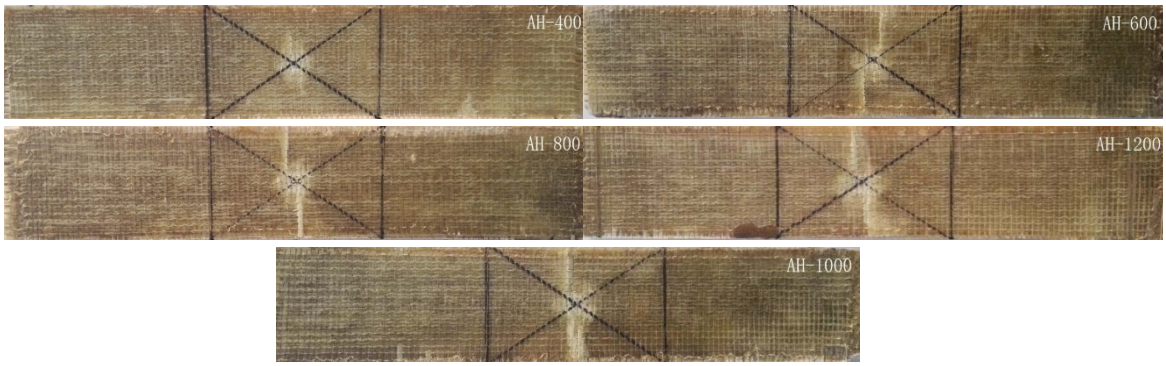


**Figure 6.** Failure mode.

*2.5. Remaining Bearing Performance Test*

Similar to the repeated four-point bending test described above, the static four-point bend test was performed on the impacted specimens in accordance with ASTM C393 [16] and GB/T 1446 [17]. Trisection loading was performed using displacement loading to 2 mm/min loading speed to load. The sample parameters are the same as Table 3, and the test loading device is shown in Figure 3.

For test piece AH-400, the deflection increased with the load point load. During the bending test loading, the damage first appeared on the load point of the upper plate or the bearing of the test piece, along with a slight cracking sound. The shear point at the point of load was maximal, the shear failure occured, and finally it peeled off from the panel, showing a sudden brittle failure. When the damage was accompanied by a huge breaking sound, the core material split in the longitudinal direction, and the entire sandwich structure failed. The AH-600 test piece was first layered at the interface with the impact-damaged panel-wood core joint interface, and the upper point of loading buckling, along with the crisp sound, the core material split, the panel peeling, still showed a sudden fragile damage. With the continuous increase of impact energy, the bending failure mode of the paulownia wood sandwich beams began to change. Such as AH-800, AH-1000 and AH-1200, the specimen bending deformation was significant, the first impact occurred at the impact point of failure, and then the formation of similar plastic hinge mechanism, the panel folds serious, the core material eventually broke due to bending deformation. The sandwich beam structure failed due to peeling of the core material and the panel. The failure mode is shown in Figure 7.

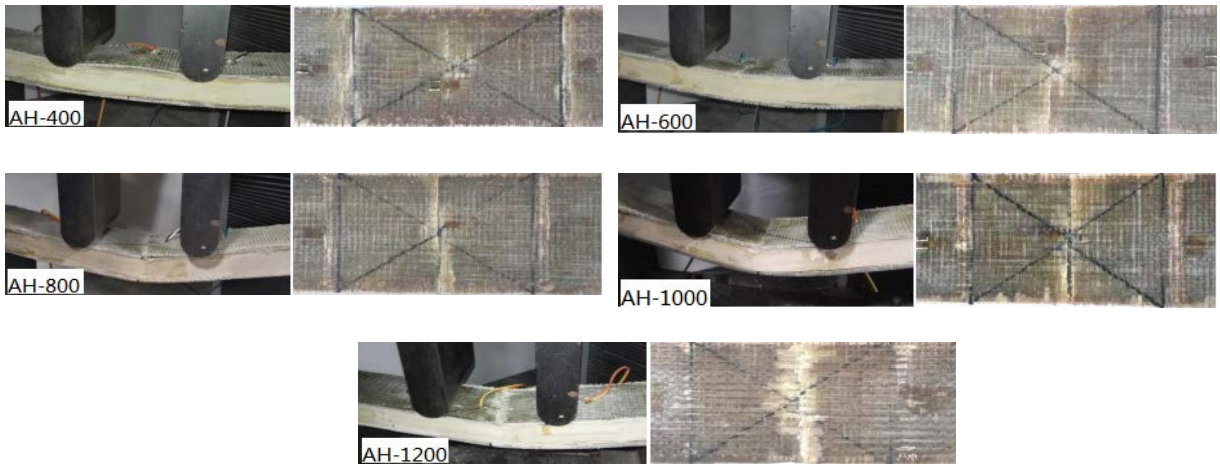


**Figure 7.** Bend test failure mode under different energy.

## 3. Analysis of Test Results

### *3.1. Analysis of Results of Four-Point Bending Test*

The load-strain curve is shown in Figure 8. In the first loading, the strain and the load show a linear relationship. After the unloading, the micro strain of the specimen decreases rapidly, but there is still a residual deformation, which is consistent with the partial recovery of the test phenomenon. In the second loading, the load-strain is presented. The linear relationship has a significant change from the first loading, reflecting that the damage of the specimen during secondary loading has expanded, and the residual deformation after unloading has been increased compared to the first time. In the third loading, the length of the load-strain linear relationship has been shortened to reflect the repeated loading and unloading of the test piece. The time damage accumulates significantly, and the strength and stiffness of the test piece decrease significantly.

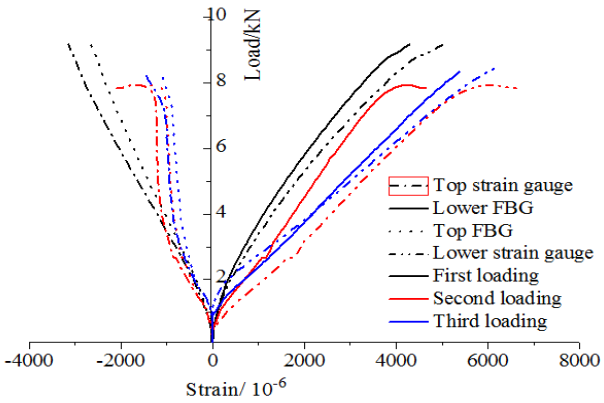


**Figure 8.** Three loading force-FBG/strain curve.

Since FBG is laid in unsaturated polyester resin, the resin shrinks after solidification, making the specimen micro-strain. The comparison between the FBG sensor's measured micro-strain and the strain gauge shows that the measured strain data of the strain gauge is slightly larger than the FBG measured conversion data. It can be considered that the length of the strain gauge distance neutralization axis is greater than the length of the FBG distance neutralization axis under the same moment of section under the bending moment load. The FBG can still work well after three times of loading and unloading, and the internal damage can be monitored in real time, indicating that the FBG has good repeatability. The test specimens are in the elastic phase during the repeated three loadings. The linearity of the load-strain curve slope of FBG is better than the linearity of the load-strain curve of strain gauges. Considering that the strain gauges arranged on the surface of the test specimen are susceptible to external environmental factors, the FBG buried inside the panel is protected. So the linearity is higher, the data is more accurate, and it can better reflect the internal strain of the specimen.

### *3.2. Analysis of Impact Test Results*

The results during the impact are shown in Table 4.

**Table 4.** Results of low-velocity impact.

| Drop height(mm) | Impact energy(J) | Impact speed(m·s$^{-1}$) | Maximum impact(kN) | Absorb energy(J) |
|---|---|---|---|---|
| 400 | 21.56 | 2.53 | 3.09 | 0.27 |
| 600 | 32.34 | 3.15 | 4.36 | 1.27 |
| 800 | 43.12 | 3.68 | 4.44 | 2.16 |
| 1000 | 53.90 | 4.23 | 4.96 | 4.34 |
| 1200 | 64.68 | 4.51 | 5.17 | 4.96 |

As the impact height increases, the total energy absorbed also increases. There is a threshold value for impact damage. When the impact energy is lower than the threshold energy, the component is in the elastic stage during the impact process. There is no plastic deformation and the total energy absorbed is small. When the impact energy is higher than the threshold energy, the load-displacement curve enters the bending stage. The test piece has a certain degree of plastic deformation during the impact and consumes a lot of energy, which leads to a rapid increase in the total energy absorbed.

The energy-displacement curve under low-speed impact is shown in Figure 9.

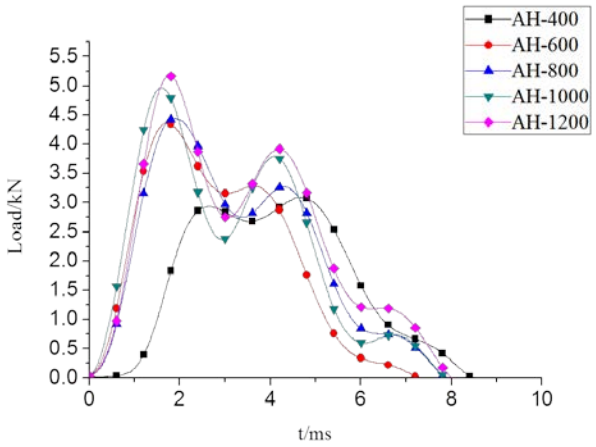


**Figure 9.** Energy - displacement curve with different impact energy.

There are two different peaks in the whole impact process. When the impact energy is small, the drop hammer touches the surface of the panel of the specimen and quickly rebound. The panel mainly undergoes elastic deformation and there is almost no loss of energy, making the first impact and the second impact almost the same. In the same way, as the energy increases, the plastic deformation occurs in the upper panel, and the plastic deformation absorbs a large amount of energy, so that the impact force during the secondary impact is smaller than the peak force of the first impact and the difference between the two peak forces is getting bigger.

When the impact energy is low, the strain-time curves of the AH-400 and AH-600 specimens across the upper and lower panels FBG and strain gauges are shown in Figure 10(a). Since the ordinary strain gauge is on the surface of the specimen, the stress wave arrives first, and the time point at which the strain peak of the strain is measured by the FBG sensor is slightly slower than that of the normal strain gauge. However, it can capture the strain change at the moment of impact and better reflect the inside of the panel. The law of strain changes.

As the impact energy increases, the strain-time curve of the AH-800 specimens across the upper and lower panels FBG and strain gauges is shown in Figure 10(b). Compared to the AH-400 and AH-600 specimens, the residual stress measured by the FBG of the AH-800 specimen is larger, indicating that the internal damage was further increased. Therefore, FBG is very sensitive to the internal force of the test piece and can detect internal damage in time.

When the specimen under high energy impact, AH-1000, AH-1200 specimen across the upper and lower panels FBG and strain gauge measured strain-time curve shown in Figure 10 (c). There is a large residual strain value after the impact of the strain gauge measured across the middle and upper surface, and the plastic deformation of the surface specimen is large, which is consistent with the severe tearing of the panel and the depression of the core material in the test phenomenon.

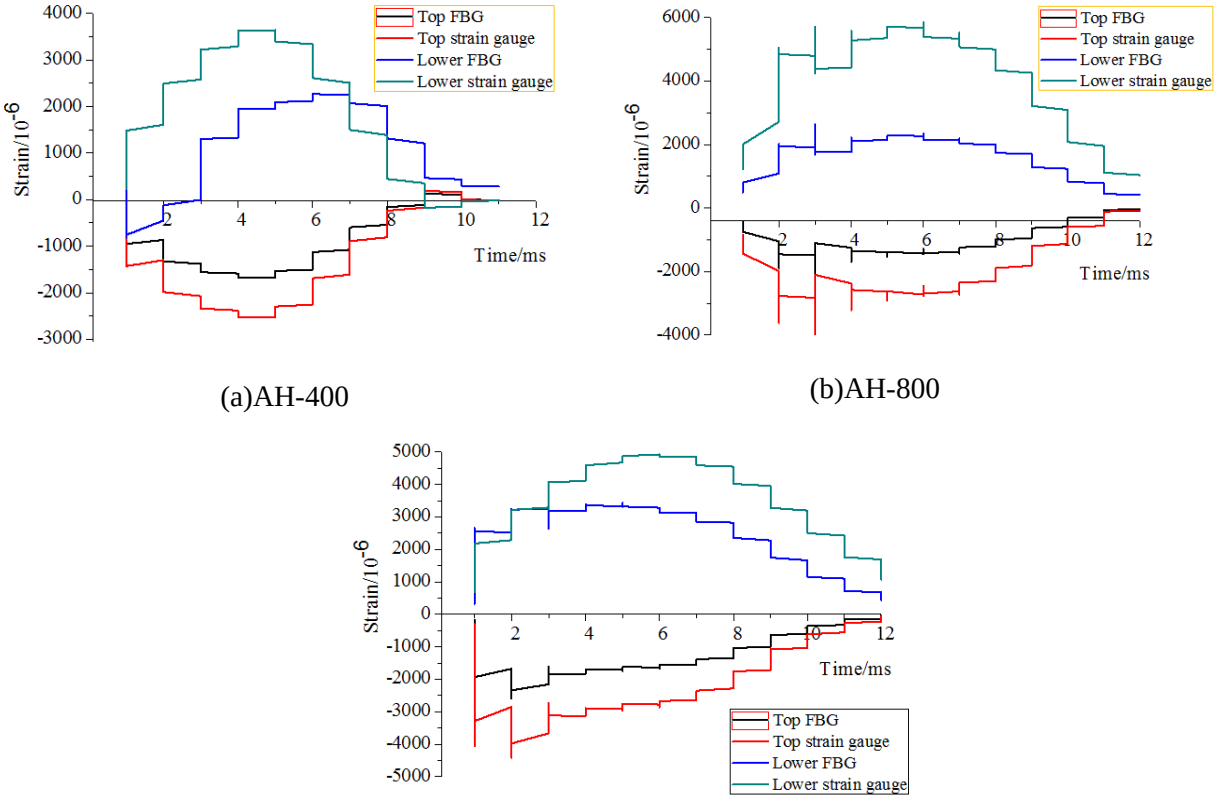


(a)AH-400 (b)AH-800

(c)AH-1200

**Figure 10.** Force-FBG/strain curve in the impact test.

3.3. *Residual Bending Performance Analysis*

In the four-point bending test of the residual bending strength, the load-displacement curve of the test piece is shown in Figure 11. It can be seen from the figure that a similar to the destruction of the elastic material, the initial load stage has an approximately linear elastic portion, and the curve suddenly drops after reaching the peak load, with obvious brittleness, such as AH-400 and AH-600. When the impact energy is large, the curves have obvious horizontal segments, such as AH-800, AH-1000 and AH-1200, which show obvious plasticity. Consistent with the test destruction described in Figure 11.

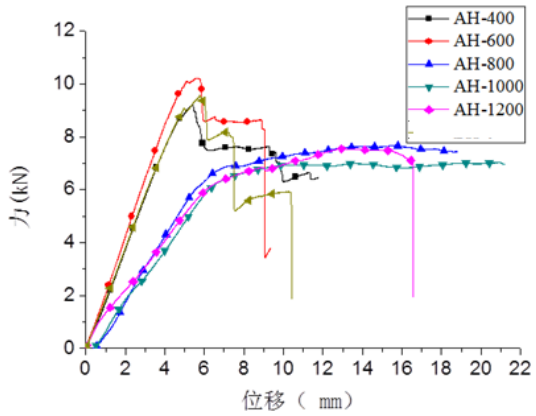


**Figure 11.** Four-point flexural load-deflection curves.

The residual bending capacity curve of the sandwich structure under different impact energy is

shown in Figure 12. The change trend of the strain measured by the FBG sensor and the strain gauge sensor on the upper and lower surfaces is approximately the same, indicating the feasibility of the FBG sensor for real-time monitoring of internal strain.

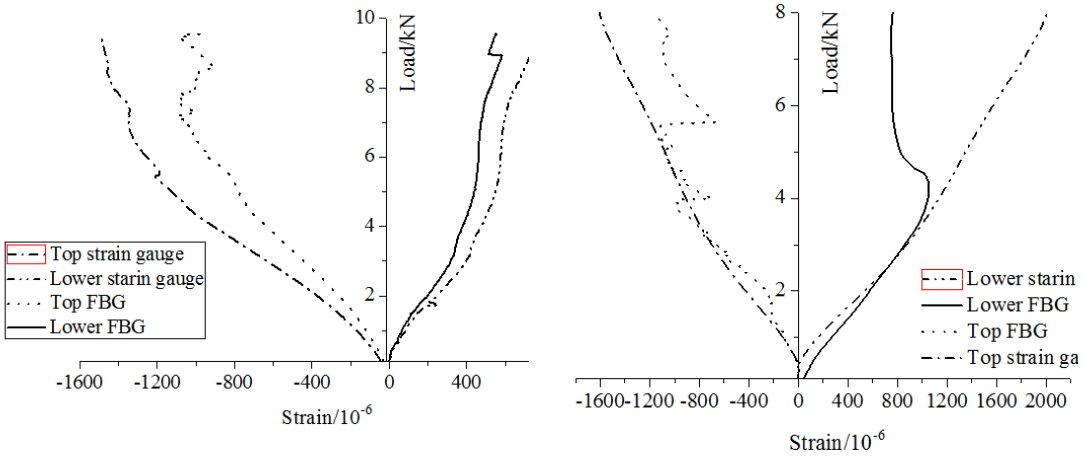


(a)AH-400 (b)AH-800

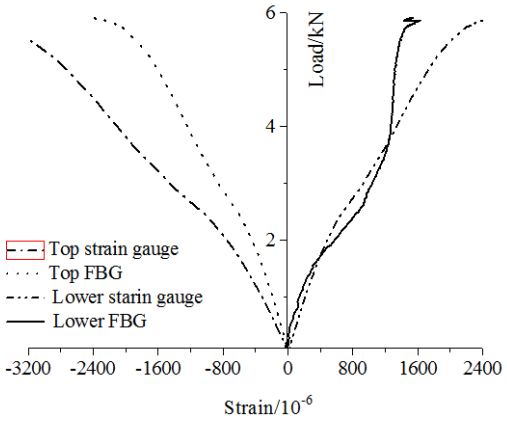


(c)AH-1200

**Figure 12.** Force-FBG/strain curves.

## 4. Summary

(1) During the repeated bending test of composite four-point bending in the composite sandwich beam, the FBG is stable after several 0-2000 micro-strain cycles and the repeatability is good. Compared with external strain gauges, the FBG sensor is buried inside the test piece, protected by FRP, and has strong resistance to external environmental disturbances. It can monitor the whole process of the loading process. It should be noted that the fiber-optic sensor pre-embedding process will have a greater impact on strain acquisition.

(2) For low-speed impact, the FBG sensor can accurately reflect the strain inside the panel. The magnitude of the residual strain after the impact reflects the degree of damage to some extent. Limited to the collection frequency of the acquisition instrument, this paper can't fully reflect the details, but it is basically used to meet the requirements for impact damage monitoring.

(3) When the impact energy is small, the internal residual deformation is small, the bending failure mode of the specimen is brittle failure. The internal residual deformation of the impact energy large specimen is large, and the failure of the specimen shows some plastic characteristics. FBG can be used to monitor the bending performance of damaged specimens, and the embedded sensor can be used to evaluate the remaining bearing capacity of specimens.

**References**

[1] Hangzhong W, Zufeng W. Rigid Polyurethane Foam Core and its Sandwich Structure *J. Materials for mechanical engineering*, 2004, 01: p 44-46. (In Chinese)
[2] Seibert H. Applications for PMI foam in aerospace sandwich structures *J. Reinforced Plastics*, 2006 (1): p 44-88.
[3] Yuming J, Quanming H. Application of Foam Sandwich Structure in Aircraft Secondary Load-Carrying Structure *J. Aeronautical manufacturing technology*, 2009 (S1): p 8-12. (In Chinese)
[4] Hongwei Z, Shuo T. Research on impact damage of composite laminates *J. Journal of Civil Aviation University of China*, 2012, 30(4): pp 11. (In Chinese)
[5] Sutsui H, Kawamata A, Sanda T, Takeda N. Detection of impact damage of stiffened composite panels using embedded small-diameter optical fibres *J. Smart Mater Struct*, 2004, 13:p 1284-1290.
[6] Bang G, Tao Y. Research on impact damage of composite laminates *J. Journal of Civil Aviation University of China*, 2009(6): p 67-71. (In Chinese)
[7] Murukeshan V M, Chan P Y, Ong L S, etal. Cure monito-ring of smart composites using Fiber Bragg Grating based em-bedded sensors *J. Sensors and Actuators*, 2000, 79 (2): p 153-161.
[8] Feifei Y, Shizhu T. Experimental study on the fabrication and measurement of long-gauge fiber bragg grating *J. Journal of Suzhou University of Science and Technology* (Engineering and Technology), 2017, 30(1): p 7-12. (In Chinese)
[9] Anderson T, Madenci E. Experimental advestigation of low-velocity impact characteristics of sandwich composites *J. Composite structures*, 2000, 50 (3): p 239-247.
[10] Guangcheng Z, Zhen H. Low-velocity impact experiment and analysis of sandwich structure composites *J. Acta Materiae Compositae Sinica*, 2012, 29(4): p 14-17. (In Chinese)
[11] Hazizan MA, Cantell WJ. The low velocity impact response of foam-based sandwich structures *J. Composite part B: Engineering*, 2000, 33(3)p 193-204.
[12] Ruixiang B, Haoran C. Adances of study on residual strength of delaminated composite sandwich plates after low velocity impact *J. Advances in mechanics*, 2002, 32(3): p 402-414. (In Chinese)
[13] Dariushi S, Sadighi M. A study on flexural property of sandwich structures with Fiber/Metal Laminate face sheets *J. Applied Composite Materials.* 2013, 20(5): p 839-855.
[14] B/T 1455-88, *Test method for shear properties of sandwich constructions or cores* [S]. (in Chinese)
[15] Standard Test Method for Tensile Properties of Polymer Matrix Composite Materials *J. Annual Book of ASTM Standards*, 2008.
[16] ASTM. C393-00 Standard Test Method for Flexural Properties of Sandwich Constructions [S]. US: *American Society for Testing and Materials*, 2000.
[17] GB/T 1446-2005. *Test method for flexural properties of sandwich constructions* [S]. China Architecture & Building Press, 2005. (In Chinese)
[18] ASTM. D7136 Standard test method for measuring the damage resistance of a fiber-reinforced polymer matrix composite to a drop-weight impact event[S]. US: *American Society for Testing and Materials*, 2007.